Electronic Supplementary Material (ESI) for ChemComm.

Supporting Information

A Versatile Two-Photon Fluorescent Probe for Ratiometric Imaging *E. Coli* β-Galactosidase in Live Cells and *in Vivo*

Xue-Xiang Zhang, Hao Wu, Peng Li, Zong-Jin Qu, Ming-Qian Tan, and Ke-Li Han*

Contents

Materials

Unless otherwise stated, all reagents were obtained from commercial source of analytical reagent grade and used without further purification. *Escherichia coli* β-galactosidase (β-gal, 400 U mg^{-1}) was purchased from J&K Chemical. Phosphate buffer saline (PBS) was aqueous solution containing 100 mM phosphate, 0.2 g L^{-1} KCl, 8 g L^{-1} NaCl. In situ β-gal staining kit was purchased from Beyotime Biotechnology Corporation (Shanghai, China). Cell Counting Kit-8 (CCK-8) was purchased from Dojindo Corporation (Shanghai, China). Matrigel was purchased from Becton, Dickinson and Company (USA). pCMV-lacZ plasmids were purchased from Clontech Laboratories, Inc. (USA) and then we commissioned TaKaRa Biotechnology Co., Ltd. (Dalian, China) to accomplish the plasmid propagation. Transfection reagent in vivo-jetPEI was purchased from Polyplus Transfection SA (France).

Instruments

All synthesis reactions were performed in flame-dried apparatus with magnetic stirring. ^{1}H and ^{13}C NMR spectra were taken on a nuclear magnetic resonance spectrometer (Bruker, Germany) at room temperature with TMS as an internal standard for chemical shifts in parts per million. High resolution mass spectra and analytical HPLC were recorded on a UFLC/MS spectrometry system, namely 6540UHD Accurate Mass Q-TOF LC/MS (Agilent, USA). Absorption spectra were obtained with a Lambda 35 UV/VIS spectrometer (PerkinElmer, USA), and the corrected fluorescence spectra were measured with a FluoroMax-4 Spectrofluorometer (HORIBA Jobin Yvon, France).

Synthesis and Characterization of Compounds

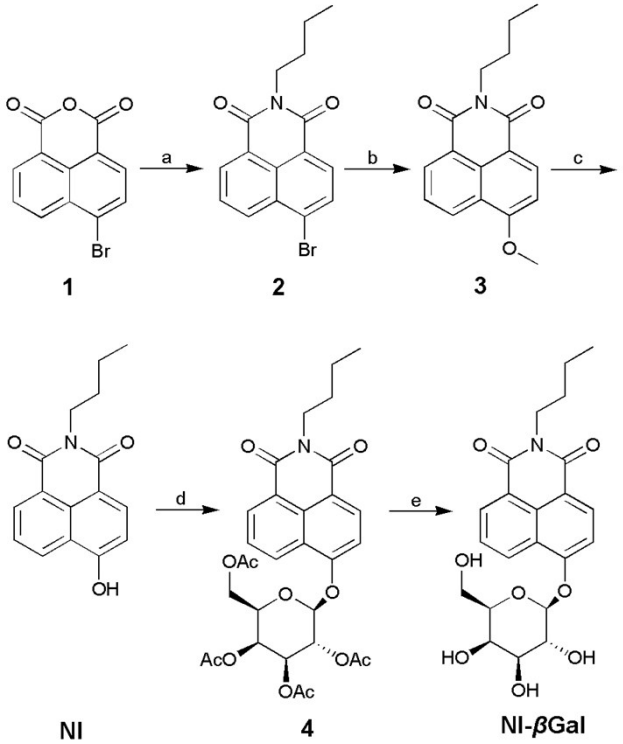

Scheme S1. Synthesis of probe NI-βGal. Reagents and conditions: (a) n-butylamine, ethanol, 68 °C; (b) CH_3ONa, $CuSO_4{\cdot}5H_2O$, CH_3OH, reflux; (c) HI, reflux; (d) 2,3,4,6-tetra-*O*-acetyl-α-D-galactopyranosyl-bromide, acetonitrile, 70 °C; (e) CH_3ONa, CH_3OH, rt, then HCl, rt.

4-bromo-*N*-butyl-1,8-naphthalimide (2). 4-bromo-1,8-naphthalic anhydride (**1**) (10.90 g, 39.0 mmol) and n-butylamine (13.9 mL, 142.0 mmol) were dissolved in 150 mL of ethanol, and the solution was stirred at 68 °C for 15 h. After completion of the reaction, solvent was evaporated under reduced pressure. The residue was purified by column chromatography on silica gel with petroleum ether-ethyl acetate (20:1, v/v) as eluent to afford compound **2** as a pale yellow solid (10.3 g, 78.8%). ^{1}H NMR (500 MHz, $CDCl_3$) δ 8.65 (dd, *J* = 7.3, 1.1 Hz, 1H), 8.56 (dd, *J* = 8.5, 1.1 Hz, 1H), 8.41 (d, *J* = 7.9 Hz, 1H), 8.04 (d, *J* = 7.9 Hz, 1H), 7.84 (dd, *J* = 8.5, 7.3 Hz, 1H), 4.19 – 4.16 (m, 2H), 1.75 – 1.69 (m, 2H), 1.45 (h, *J* = 7.5 Hz, 2H), 0.98 (t, *J* = 7.4 Hz, 3H).

4-methoxyl-*N*-butyl-1,8-naphthalimide (3). A mixture of 4-bromo-N-butyl-1,8-naphthalimide (**2**) (7.50 g, 22.6 mmol), CH_3ONa (21.30 g, 394.0 mmol) and $CuSO_4{\cdot}5H_2O$ (0.65 g, 2.6 mmol) in 100 mL of CH_3OH were refluxed for 6 h. After completion of the reaction, solvent was evaporated under reduced pressure. Then CH_2Cl_2 and saturated aqueous NaCl solution were added to the residue. The organic layer was extracted and dried over anhydrous Na_2SO_4, which was removed by filtration. The filtrate was then concentrated under reduced pressure. The crude product was purified by column chromatography on silica gel using petroleum ether-ethyl acetate (15:1, v/v) as eluent to give compound **3** as a yellowish white granular powder (4.1 g, 64.1%). ^{1}H NMR (500 MHz, $CDCl_3$) δ 8.56 (dd, *J* = 7.3, 1.2 Hz, 1H), 8.52 – 8.49 (m, 2H), 7.66 (dd, *J* = 8.3, 7.4 Hz, 1H), 7.01 (d, *J* = 8.3 Hz, 1H), 4.16 (t, *J* = 7.6 Hz, 2H), 4.11 (s, 3H), 1.76 – 1.68 (m, 2H), 1.45 (h, *J* = 7.5 Hz, 2H), 0.98 (t, *J* = 7.4 Hz, 3H).

NI. A mixture of 4-methoxy-N-butyl-1,8-naphthalimide (**3**) (3.80 g, 13.5 mmol) and 57% (v/v) hydroiodic acid (170 mL) was refluxed for 12 h. After cooling, the precipitate was filtered and washed with water (30 mL × 3) while preserving the filtrate. The crude product was subjected to recrystallization using ethyl acetate (80 mL) and petroleum ether (80 mL). The crystalline solid was collected by vacuum filtration and dried under vacuum to give compound **NI** as yellow needles (1.70 g). The combined filtrate from aforementioned filtrations was concentrated under reduced pressure and the resulting residue was purified by column chromatography on silica gel using petroleum ether-ethyl acetate (10:1, v/v) as eluent to give compound **NI** as yellow needles (1.20 g). The overall yield was 79.8%. ^{1}H NMR (500 MHz, DMSO) δ 11.85 (s, 1H), 8.50 (dd, *J* = 8.3, 1.3 Hz, 1H), 8.43 (dd, *J* = 7.3, 1.3 Hz, 1H), 8.33 (d, *J* = 8.2 Hz, 1H), 7.73 (dd, *J* = 8.3, 7.2 Hz, 1H), 7.14 (d, *J* = 8.2 Hz, 1H), 4.04 – 3.98 (m, 2H), 1.67 – 1.53 (m, 2H), 1.35 (h, *J* = 7.4 Hz, 2H), 0.94 (t, *J* = 7.4 Hz, 3H). ^{13}C NMR (126 MHz, DMSO) δ 163.537, 162.872, 160.111, 133.355, 130.932, 129.054, 128.711, 125.397, 122.275, 121.698, 112.543, 109.837, 39.296, 29.683, 19.754, 13.625. HRMS (ESI$^+$): m/z calcd for $(M + H)^+$, 270.1125; found, 270.1141.

NI-βGal Tetraacetate (4). A three-necked, round-bottomed flask equipped with nitrogen inlet adapter and reflux condenser was charged with NI (0.90 g, 3.3 mmol), 2,3,4,6-tetra-*O*-acetyl-α-D-galactopyranosyl-bromide (2.10 g, 5 mmol), K_2CO_3 (1.34 g, 9.7 mmol) and acetonitrile (15 mL, HPLC grade). The reaction was stirred at 70 °C under N_2 atmosphere for 4 h. After cooling to room temperature, the mixture was poured into water followed by filtration. Washed the filter residue three times with water and then dissolved it in ethyl acetate. Then the solvent was evaporated under reduced pressure, and the residue was purified by column chromatography on silica gel with petroleum ether-ethyl acetate (10:1, v/v) as eluent to afford compound **4** as a white solid(1.21 g, 60.4%). ^{1}H NMR (500 MHz, $CDCl_3$) δ 8.62 (dd, *J* = 7.3, 1.2 Hz, 1H), 8.54 (d, *J* = 8.2 Hz, 1H), 8.45 (dd, *J* = 8.4, 1.2 Hz, 1H), 7.75 (dd, *J* = 8.4, 7.3 Hz, 1H), 7.24 (d, *J* = 8.3 Hz, 1H), 5.75 (dd, *J* = 10.5, 7.9 Hz, 1H), 5.56 (d, *J* = 3.4 Hz, 1H), 5.39 (d, *J* = 7.9 Hz, 1H), 5.24 (dd, *J* = 10.5, 3.4 Hz, 1H), 4.33 – 4.20 (m, 3H), 4.17 (t, *J* = 7.6 Hz, 2H), 2.23 (s, 3H), 2.11 (s, 3H), 2.07 (s, 3H), 2.06 (s, 3H), 1.76 – 1.66 (m, 2H), 1.45 (h, *J* = 7.4 Hz, 2H), 0.98 (t, *J* = 7.3 Hz, 3H). ^{13}C NMR (126 MHz, $CDCl_3$) δ 170.083, 169.956, 169.774, 169.429, 163.938, 163.383, 157.176, 132.234, 131.558, 129.090, 128.035, 126.578, 123.344, 122.332, 117.182, 108.779, 98.796, 71.481, 70.308, 68.275, 66.726, 61.308, 39.926, 30.028, 20.560, 20.465, 20.436, 20.375, 20.164, 13.642. HRMS (ESI$^+$): m/z calcd for $(M + H)^+$, 600.2076; found, 600.2085.

NI-βGal. A mixture of NI-βGal Tetraacetate (**4**) (0.62 g, 1.0 mmol), CH_3ONa (0.11 g, 1.0 mmol) and methanol (40 mL) was stirred at room temperature for 3 h and then neutralized with hydrochloric acid. The reaction mixture was filtered and the filtrate was then concentrated under reduced pressure. The crude product was subjected to twice recrystallization using methanol to give compound **NI-βGal** as a white sheet-like solid (0.24 g, 53.8%). ^{1}H NMR (500 MHz, DMSO) δ 8.69 (dd, *J* = 8.4, 1.2 Hz, 1H), 8.47 (dd, *J* = 7.3, 1.2 Hz, 1H), 8.40 (d, *J* = 8.3 Hz, 1H), 7.82 (dd, *J* = 8.4, 7.3 Hz, 1H), 7.45 (d, *J* = 8.4 Hz, 1H), 5.47 (d, *J* = 5.3 Hz, 1H), 5.22 (d, *J* = 7.7 Hz, 1H),

4.97 (d, *J* = 5.7 Hz, 1H), 4.71 (t, *J* = 5.5 Hz, 1H), 4.62 (d, *J* = 4.6 Hz, 1H), 4.01 (t, *J* = 7.4 Hz, 2H), 3.88 – 3.81 (m, 1H), 3.81 – 3.74 (m, 2H), 3.68 – 3.46 (m, 3H), 1.68 – 1.52 (m, 2H), 1.34 (h, *J* = 7.4 Hz, 2H), 0.92 (t, *J* = 7.4 Hz, 3H). ^{13}C NMR (126 MHz, DMSO) δ 163.506, 162.843, 158.225, 132.758, 131.073, 128.861, 128.507, 126.313, 122.986, 121.779, 115.174, 109.689, 101.078, 75.906, 72.956, 70.255, 68.082, 60.318, 39.214, 29.683, 19.783, 13.685. HRMS (ESI$^+$): m/z calcd for (M + H)$^+$, 432.1653; found, 432.1651.

Absorption and fluorescence spectra

Absorption spectra were obtained with a 1.0-cm quartz cuvette, and fluorescence spectra were obtained with a Xenon lamp and 1.0-cm quartz cuvette. 3 mL of NI-βGal or NI (final concentration, 3 μM) in PBS buffer (100 mM, 0.3% DMSO, pH 7.4) was added to 1.0-cm quartz cuvette and then the absorption and fluorescence spectra were scanned and recorded (Fig. S1 and S2). The fluorescence intensity was measured upon excitation at 365 nm and 445 nm for NI-βGal and NI, respectively. As regards the time-dependent absorption and fluorescence spectra, 6 units of β-gal (final concentration, 5 μg mL^{-1}) was added to NI-βGal (final concentration, 3 μM) in PBS buffer (100 mM, 0.3% DMSO, pH 7.4) at room temperature, and immediately the mixed solution was subjected to serial absorption or fluorescence spectra scanning over the course of 30 min. The time-dependent fluorescence spectra were obtained upon excitation at 395 nm.

Table S1. Photophysical properties of NI-βGal and NI.

Compound	λ_{abs}[a]	λ_{fl}[b]	$\Delta\lambda$[c]	ε[d]	Φ[e]
NI-βGal	365	440	75	13,000	0.94
NI	445	545	100	11,000	0.06

[a] λ_{max} of absorption spectra in nm. [b] λ_{max} of fluorescence spectra in nm. [c] Stokes shift in nm. [d] Molar extinction coefficients in M^{-1} cm^{-1} at the absorption maximum. [e] Relative fluorescence quantum yield with 0. 05 M quinine sulfate in 0.1 M H_2SO_4 (0.62) as a reference.[1]

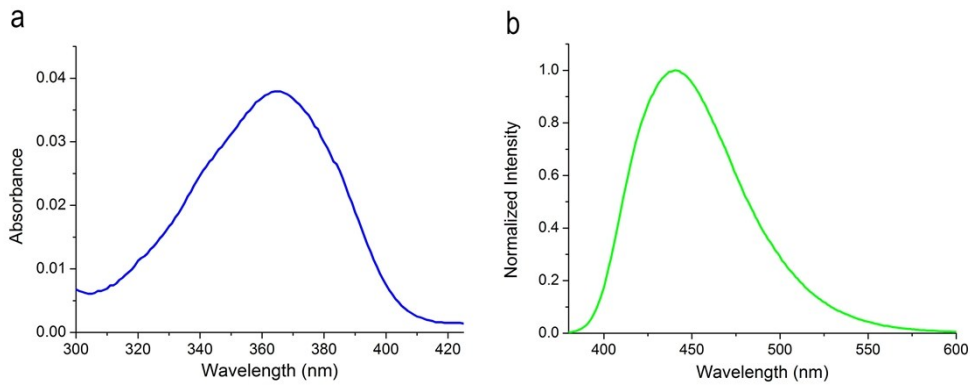

Fig. S1. Absorption (a) and normalized fluorescence (b) spectra of NI-βGal.

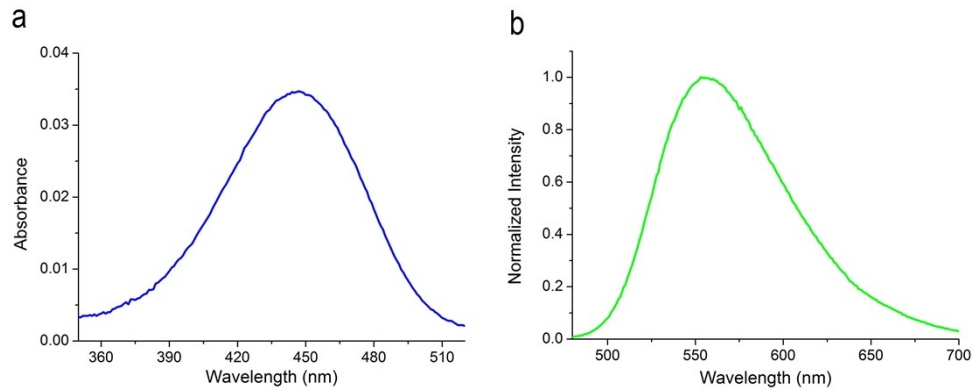

Fig. S2. Absorption (a) and normalized fluorescence (b) spectra of NI.

p*K*a measurement

All pH measurements were made with a STARTER2100 pH meter (Ohaus, USA). At a series of pH (2.0, 3.0, 3.5, 4.1, 4.5, 5.0, 5.3, 5.4, 5.7, 5.8, 5.9, 6.1, 6.2, 6.4, 6.6, 6.8, 7, 7.4, 7.6, 6.0, 9.0, 10.0), the fluorescence spectra of NI (final concentration, 15 μM) in PBS buffer (100 mM, 0.3% DMSO, 1.5% ethanol) were obtained upon excitation at 445 nm (Fig. S3a), and then intensities at 545 nm was used to plot the F-pH curve (Fig. S3b).

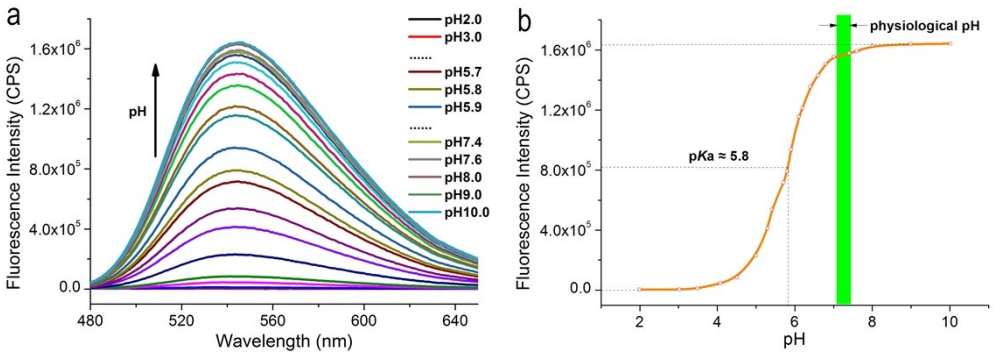

Fig. S3. (a) pH-dependent fluorescence spectra of NI. (b) The dependence of fluorescence intensity of NI in PBS buffer (100 mM, 0.3% DMSO, 1.5% ethanol) at 545nm on pH (λ_{ex} = 445nm).

Determination of fluorescence quantum yield

Fluorescence quantum yields Φ_{fl} (relative values) of NI-βGal and NI were determined using 0. 05 M quinine sulfate (0.62 in 0.1 M H_2SO_4)[1] as a reference at an excitation wavelength of 390 nm. The quantum yield was calculated using the following equation:[2]

$$\Phi_s = \frac{F_s}{F_r} \times \frac{1 - 10^{-A_r}}{1 - 10^{-A_s}} \times \Phi_r$$

where the subscripts *s* and *r* denote the sample and reference, respectively, *F* is the integrated fluorescence intensity under fluorescence emission spectrum, A is the absorbance at the excitation wavelength.

Tracing the conversion of NI-βGal to NI by HPLC analysis.

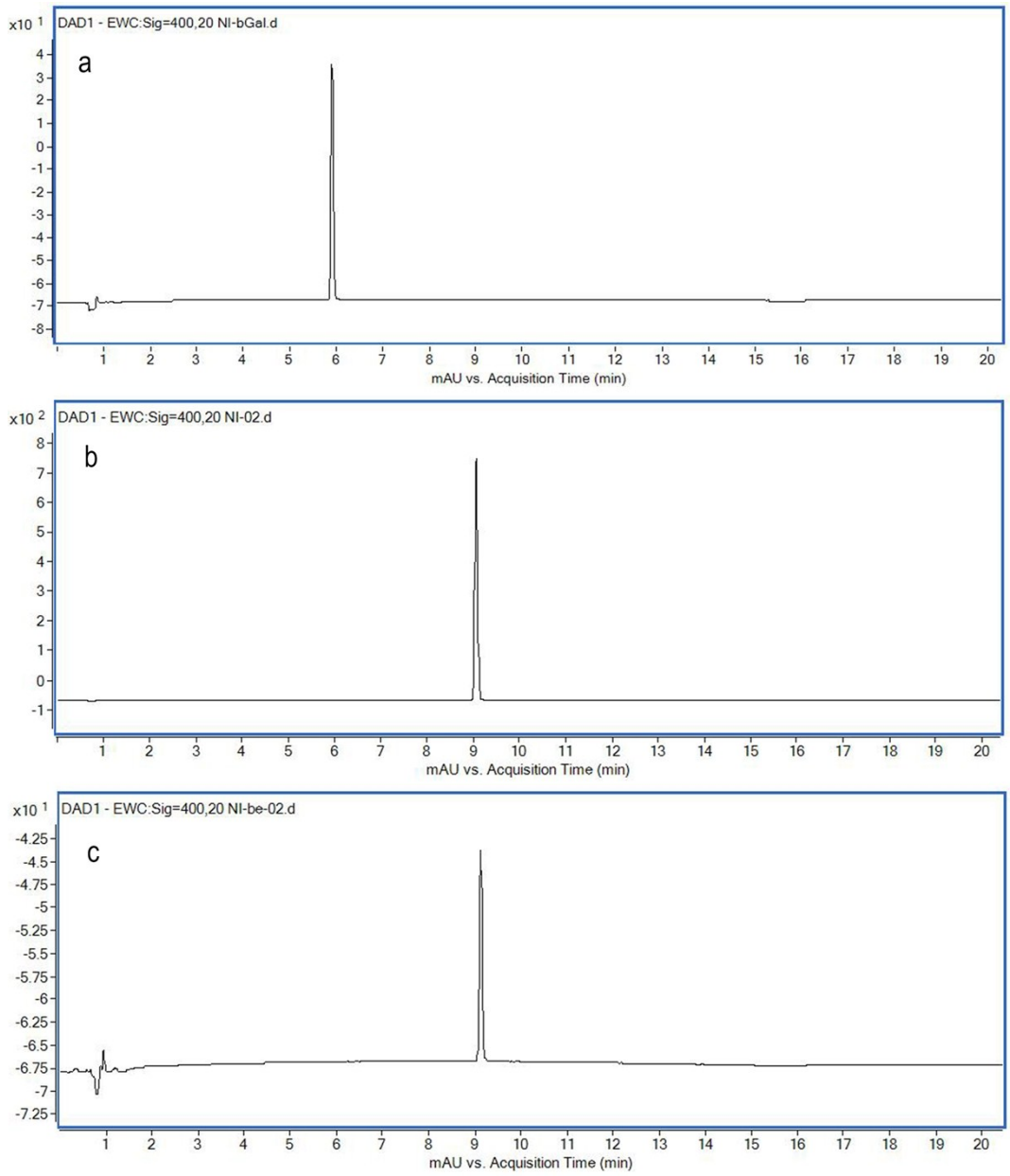

Fig. S4. HPLC traces of NI-βGal (a), NI (b) and the reaction product between NI-βGal and β-gal (c). An isocratic condition was used: 200 µL min^{-1} flow rate, 5% A to 95% A over 15 min, detected at 400 nm. Solvent A is water with 0.1% formic acid and solvent B is acetonitrile. The reaction was carried out for 2 h at room temperature in pure water. Peaks at 5.9 min and 9.1 min correspond to NI-βGal and NI, respectively.

Enzymatic kinetic study

The enzymatic kinetic study of β-gal/NI-βGal reaction was performed by monitoring changes in fluorescence intensity using a microplate reader Varioskan Flash (Thermo Fisher Scientific, USA). All measurements were carried out in PBS buffer (100 mM, 5% DMSO, pH 7.4) at 37 °C in triplicate. The final volume of the mixed solution was 200 μL (final concentration: 0.058 μg mL^{-1} for β-gal). Briefly, pre-incubated enzyme solution was added to NI-βGal of a series of concentrations (from 0 to 100 μM) to initiate the reaction. Immediately, the fluorescence emission at 560 nm was measured using a plate reader upon excitation at 445 nm for 25 min to determine the formation of NI. The initial reaction rates were determined by the data within a linear response range. Kinetic parameters (K_m, k_{cat}, k_{cat}/K_m and V_{max}) were calculated by direct fits of the data to the Michaelis-Menten Equation using a nonlinear regression via GraphPad Prism software.

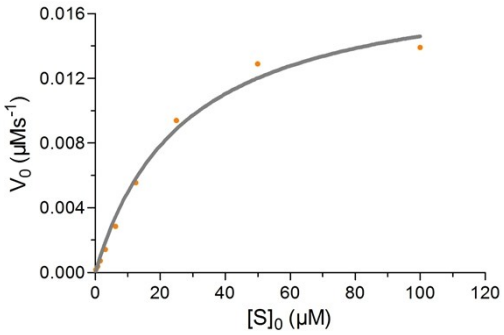

Fig. S5. Kinetic study of β-gal/NI-βGal enzymatic reaction over a NI-βGal-concentration range 0–100 μM with 0.058 μg mL^{-1} β-gal in PBS buffer (100 mM, 5% DMSO, pH 7.4) at 37 °C.

Cell culture

C6 (glioblastoma, fibroblast, rat), C6/lacZ7 (glioblastoma, fibroblast, rat) and U-87 MG cells (glioblastoma, astrocytoma, human) were purchased from American Type Culture Collection (ATCC) and cultured in H-DMEM medium supplemented with 10% fetal bovine serum (FBS), penicillin (100 units mL^{-1}) and streptomycin (100 μg mL^{-1}) in a humidified atmosphere containing 5% CO_2 at 37 °C. HL-7702 cells (liver, human) were purchased from KeyGEN BioTECH Corporation (Shanghai, China) and cultured in RPMI 1640 medium supplemented with 10% fetal bovine serum (FBS), penicillin (100 units mL^{-1}) and streptomycin (100 μg mL^{-1}) in a humidified atmosphere containing 5% CO_2 at 37 °C. C6 and C6/lacZ7 cells were maintained 24 h before imaging and then seeded in glass bottom dish (Φ20mm, Corning) at a density of 1×10^4 cells $dish^{-1}$.

Cell viability

Cell viability test was evaluated by the Cell Counting Kit-8 (CCK-8, Dojindo) test.[3] In this test, C6 cells and HL-7702 cells were seeded in 96-well plate at a density of 5×10^3 cells $well^{-1}$ and cultured for 24 h. Medium containing NI-βGal of a series of concentrations (0, 0.020, 0.039, 0.078, 0.156, 0.313, 0.625, 1.25, 2.5, 5, 10 μM for C6 cells; 0, 0.156, 0.313, 0.625, 1.25, 2.5, 5, 10, 20, 40 μM for HL-7702 cells) was used to incubate the cells for 24 h. Washed the cells with PBS buffer three times and then added 100 μL of medium

and 10 μL of CCK-8 solution, followed by incubation for 2 h. Afterwards, the optical density (*OD*) at 450 nm (630 nm as a reference) was measured using a microplate reader (Wellscan MK3, Labsystems). The cell viability was estimated according to the following equation:

$$Cell\ Viability\ (\%) = \frac{OD_{treated}}{OD_{control}} \times 100\%$$

where $OD_{control}$ is measured in the absence of NI-βGal and $OD_{treated}$ donates the intensity obtained in the presence of NI-βGal.

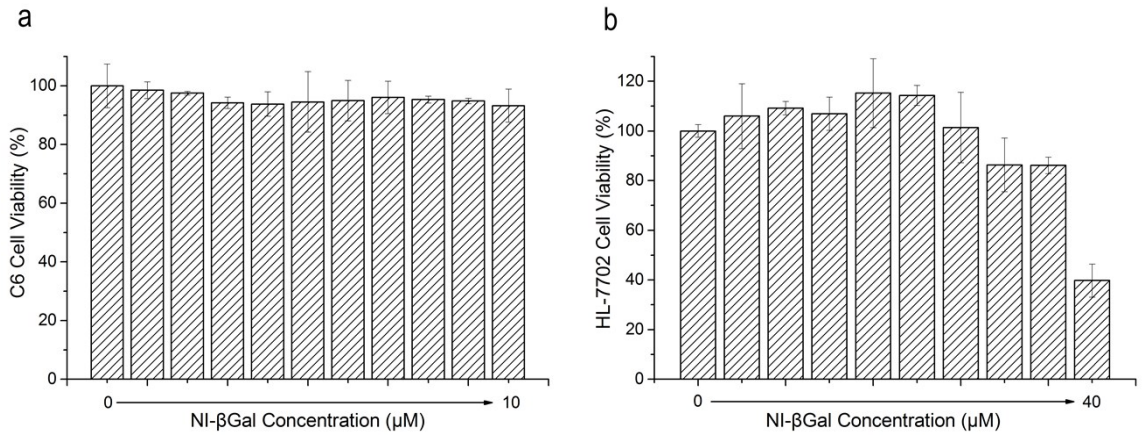

Fig. S6. Viability of (a) C6 cells and (b) HL-7702 cells in the presence of NI-βGal as measured by using CCK-8 kit. Error bars represent s.d. from a single experiment in triplicate.

Celluar fluorescence imaging

The one-photon cellular fluorescence microscopy images were captured by a FV1000 confocal laser scanning microscope (Olympus, Japan), and the two-photon cellular fluorescence microscopy images were obtained with a FV1000MPE microscope (Olympus, Japan) by exciting the probe with a mode-locked titanium-sapphire pulse laser source (MaiTai Spectra Physics, 80 MHz, 100 fs) set at a wavelength of 740 nm. Both C6 and C6/lacZ7 cells were incubated with the probe NI-βGal (10 μM) in PBS buffer (100 mM, 1% DMSO, 0.5 g L^{-1} glucose, pH 7.4) for 1 h. On the other hand, C6 and C6/lacZ7 cells incubated with PBS buffer (100 mM, 1% DMSO, 0.5 g L^{-1} glucose, pH 7.4) alone were as blank control (Fig. S8 and S9). For one-photon fluorescence imaging, the cells were excited at 488 nm with a 100 × objective lens, and the collection range of emission channel was set as 520−560 nm. For two-photon fluorescence imaging, the cells were excited at 740 nm with a 100 × objective lens, and then fluorescence in blue channel (420−460 nm) and yellow channel (520−560 nm) was collected.

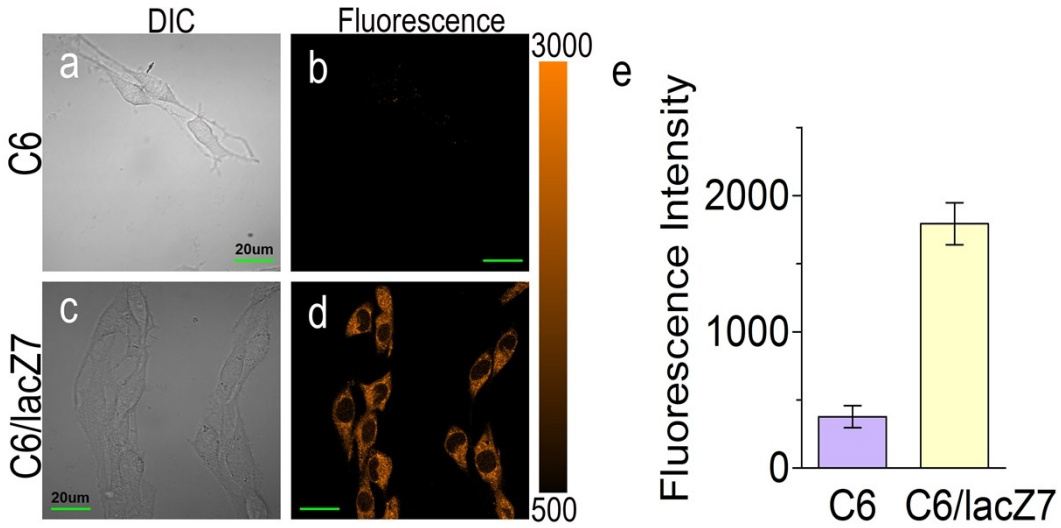

Fig. S7. (a−d) One-photon excitation fluorescence microscopic imaging of β-gal activity with NI-βGal in live C6 (a, b) and C6/lacZ7 (c, d) cells. (a, c) DIC images. (b, d) Images in fluorescence channel (520−560 nm). (e) Average fluorescence intensity values in (b) and (d). Cells were incubated with NI-βGal (10 μM) in PBS buffer (100 mM, 1% DMSO, 0.5 g L^{-1} glucose, pH 7.4) at room temperature for 1 h and then images were acquired using 488 nm excitation with a 100 × objective. Representative images from repeated experiments (n = 3) are shown. Color bar calibrates the intensity values in fluorescence channel (b and d). Scale bar = 20 μm. Error bars represent s.d.

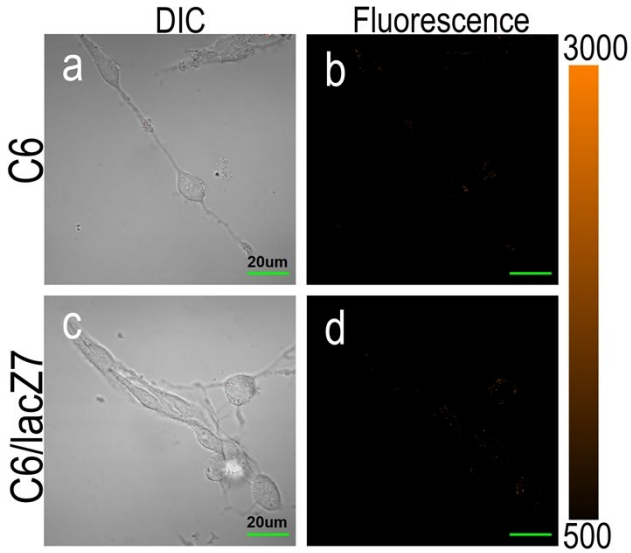

Fig. S8. (a−d) One-photon excitation fluorescence microscopic imaging of C6 (a, b) and C6/lacZ7 (c, d) cells incubated with PBS buffer (100 mM, 1% DMSO, 0.5 g L^{-1} glucose, pH 7.4) alone. (a, c) DIC images. (b, d) Images in fluorescence channel (520−560 nm). λ_{ex} = 488 nm. Color bar calibrates the intensity values in fluorescence channel (b and d). Scale bar = 20 μm.

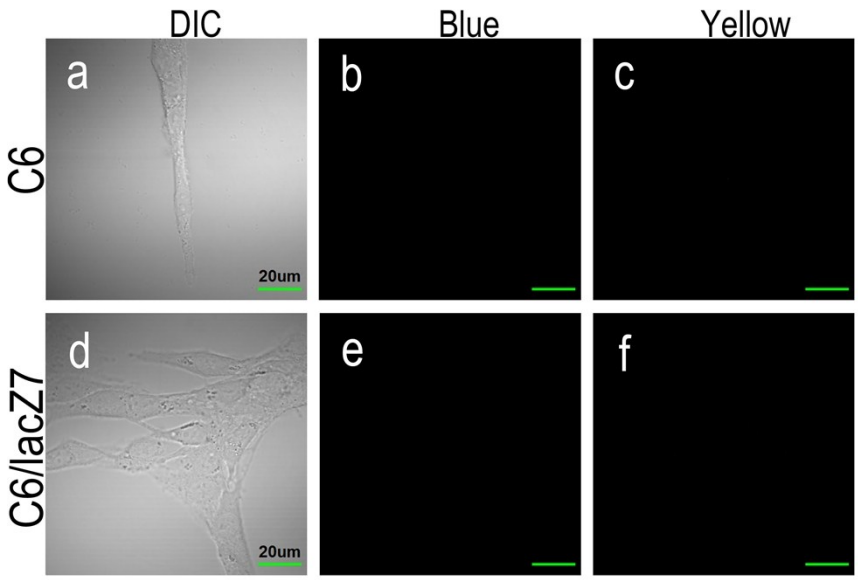

Fig. S9. (a−f) Two-photon excitation fluorescence microscopic imaging of C6 (a−c) and C6/lacZ7 (d−f) cells incubated with PBS buffer (100 mM, 1% DMSO, 0.5 g L^{-1} glucose, pH 7.4) alone. (a, d) DIC images. (b, e) Images in blue channel (420−460 nm). (c, f) Images in yellow channel (520−560 nm). λ_{ex} = 740 nm. Scale bar = 20 μm.

Conventional X-Gal assay

β-gal activity were evaluated by the in situ β-gal Staining Kit containing X-Gal. C6 and C6/lacZ7 cells were seeded in 24-well plates at a density of 1 × 10^4 cells $well^{-1}$ and incubated for 24 h. Then, the in situ β-gal Staining Kit test was executed according to the manufacturer's instructions and the cells were imaged using a Ti-S inverted microscope (Nikon, Japan) with a 20 × objective lens. As for histological analyses, the tumor tissues were cryosectioned into 10-μm thick slices and then subjected to in situ β-gal Staining Kit test, followed by imaging with a 10 × objective lens mounted in the same microscope aforementioned. Tumor slices were prepared with a CM 1100 microtome (Leica, Germany).

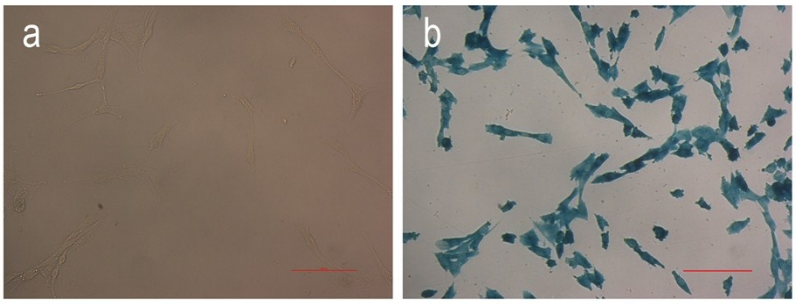

Fig. S10. Conventional X-Gal chemical assay for β-gal expression was administrated to C6 (a) and C6/lacZ7 (b) cells. Scale bar = 100 μm.

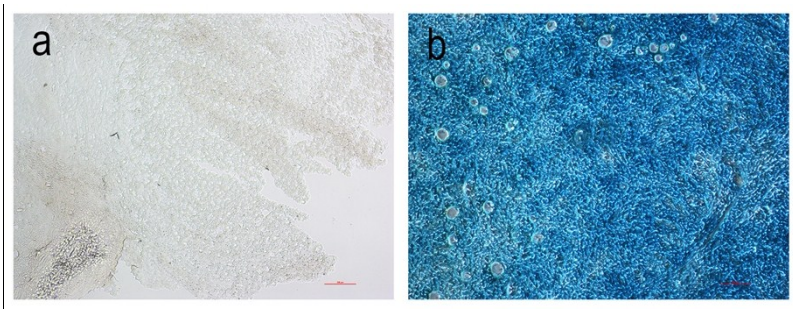

Fig. S11. Histological X-Gal staining on C6 (a) and C6/lacZ (b) tumor sections. Scale bar = 100 μm.

Tumor model

Female BALB/c-nu mice (4–6 weeks) were purchased from the Animal Center of Dalian Medical University. C6 and C6/lacZ7 cells (5×10^6) were subcutaneously implanted respectively into the left and right flanks of three mice for stable tranfection imaging, whereas U-87 MG cells (5×10^6) were subcutaneously implanted into both flanks of three other mice for transient transfection test, with a mixture of 50 μL of serum-free media and 50 μL of Matrigel for each tumor. Subsequent experiments were conducted when the tumor size reached 7 mm in diameter. All animal studies were carried out at the Specific Pathogen Free (SPF) Animal Center at the Dalian Medical University according to the animal protocols approved by the Animal Ethics Committee (AEC).

In vivo tumor transient transfection

We used in vivo-jetPEI transfection reagents to achieve the gene transfer, according to the manufacturer's instructions. Briefly, 24 μg of endotoxin-free pCMV-lacZ plasmids was mixed with a ratio of L-PEI nitrogen to DNA phosphate of 10 in 60 μL of 5% w/v glucose. After 15 min incubation at room temperature, the L-PEI/DNA mixture was injected intratumorally into the right tumors of U-87 MG-tumor-bearing mice. As blank control, the left tumors were intratumorally injected the same amount of transfection reagents containing no pCMV-lacZ plasmids. The same treatments were executed every other day and 48 h after the second treatment the mice were subjected to in vivo whole-body imaging.

In vivo whole-body imaging

The serial whole-body images of mice were obtained with the Maestro EX in vivo Imaging System (CRi, USA). The mice were anesthetized by 2% isoflurane and intratumorally injected with 50 μL of NI-βGal (100 μM) in PBS buffer (100 mM, 10% DMSO, pH 7.4). Serial fluorescence imaging was taken on a Maestro EX in vivo imaging system after injection. Fluorescence images were acquired using the following parameters: Excitation Wavelength: 455 nm; Emission Filter: 490 nm long-pass filter; Acquisition Settings: 500–720 nm in 10 nm steps; Exposure times were 500 ms. After subtracting the background autofluorescence and selecting the ROIs over the tumors, the quantified results were obtained from the multispectral fluorescence images by Maestro software (Cambridge Research & Instrumentation, Inc.). Statistical analysis was performed by Statistical Product and Service Solutions software (SPSS, Inc.).

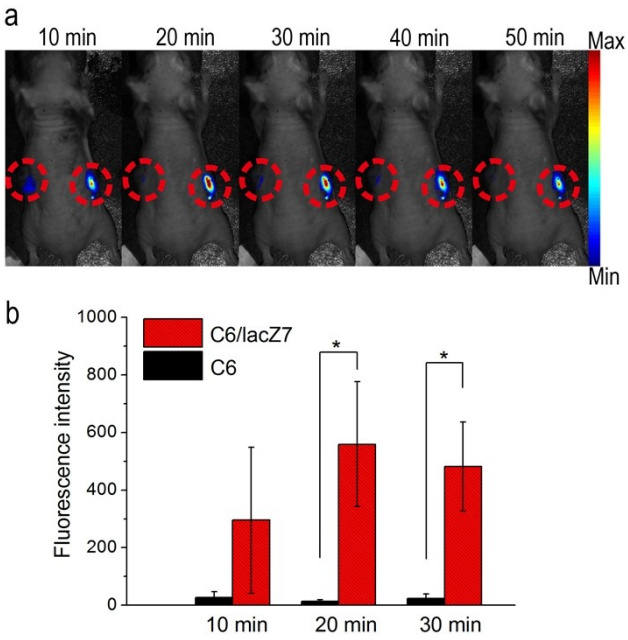

Fig. S12. (a) In vivo serial whole-body imaging of stable β-gal expression in nude mouse bearing C6 (left flank) and C6/lacZ (right flank) tumors. NI-βGal (2.2 μg) was injected intratumorally and then captured the images. Sites of the tumors were marked by red circles. λ_{ex} = 455 nm. Fluorescence aquisition: 500–720 nm. (b) Time course of in vivo activation of NI-βGal. *p < 0.05, n = 3, Student's t-test, two-tailed, error bars represent s.d.

In order to preclude the interference from possible intrinsic β-galactosidase activity of normal cells or organs, both in vivo (Fig. S13) and ex vivo (Fig. S14) control experiments were implemented. It is demonstrated that there's hardly any interference from normal mammalian cells or organs.

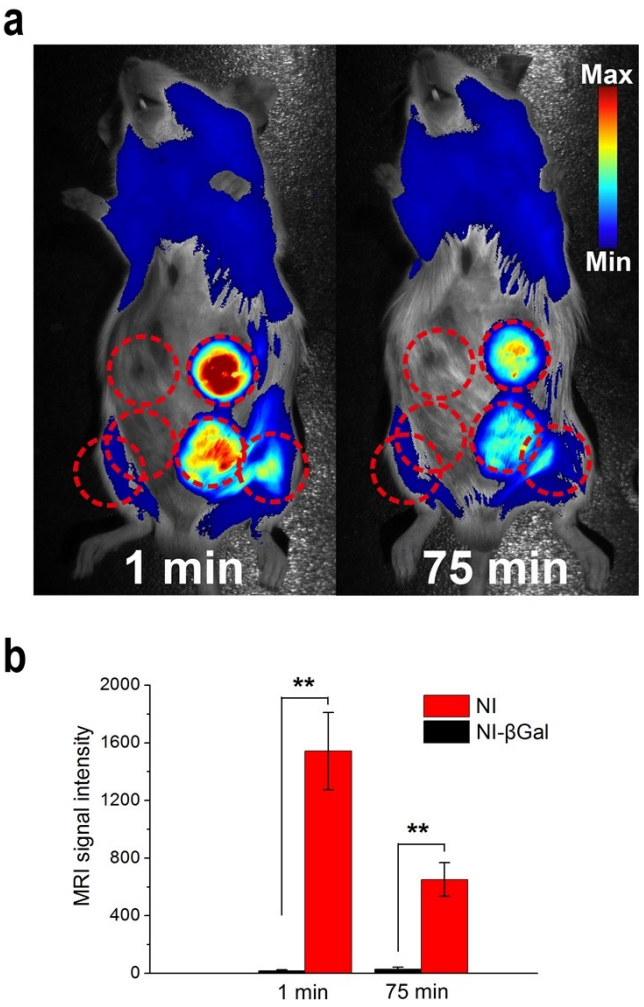

Fig. S13. (a) In vivo serial whole-body imaging of Kunming mouse after subcutaneous injection of NI-βGal (2.2 μg, 5 nmol, left flank) and NI (1.3 μg, 5 nmol, right flank). Sites of the injection were marked by red circles. λ_{ex} = 455 nm. Fluorescence aquisition: 500–720 nm. (b) Quantified results of (a). $^{**}p < 0.01$, $n = 3$, Student's t-test, two-tailed, error bars represent s.d.

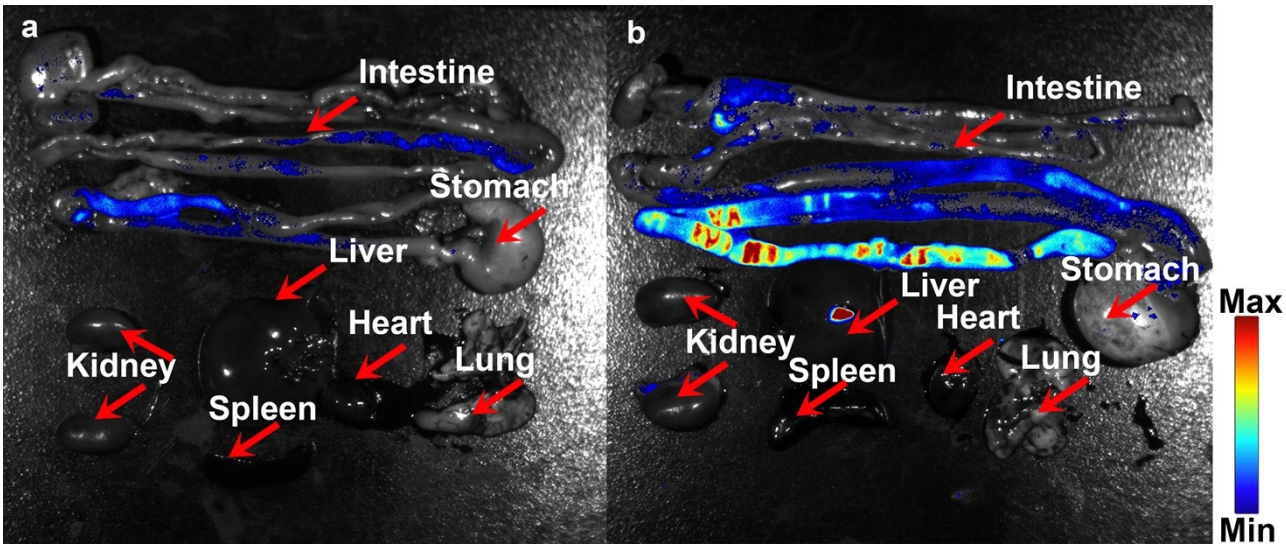

Fig. S14. Ex vivo imaging of distinct organs of Kunming mice at 0.5 h post intraperitoneal injection of (a) NI-βGal (2.2 μg, 5 nmol) or (b) NI (1.3 μg, 5 nmol). Organs were marked by red arrows. λ_{ex} = 455 nm. Fluorescence aquisition: 500–720 nm.

Colocalization

Colocalization experiments (Fig. S15–17) were conducted to show more information about our probe NI-βGal. The Pearson's colocalization coeffcients of NI-βGal and Mito-Tracker Deep Red or Lyso-Tracker Red were calculated to be 0.68 and 0.81, respectively. These results showed that NI, the hydrolysate of NI-βGal upon encounter with β-gal, was more likely to aggregate in the lysosome.

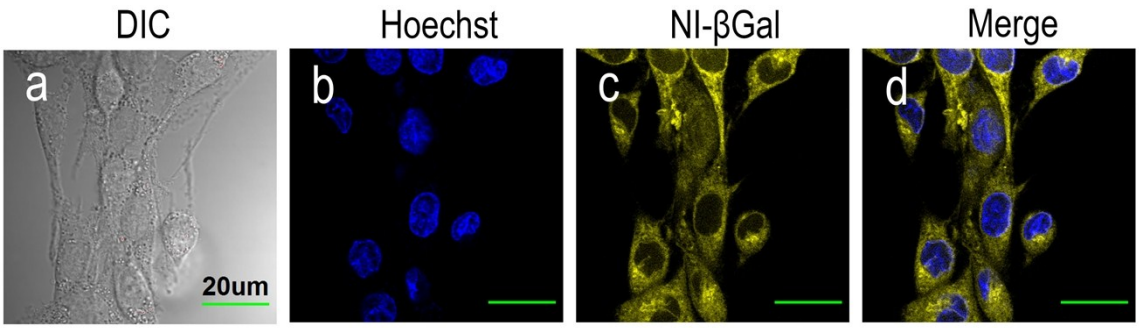

Fig. S15 Images of C6/lacZ7cells colabeled with (b) Hoechst (a commercial nucleus-staining dye) and (c) NI-βGal. (a) DIC image. (d) Merged image of (b) and (c). The excitation wavelengths for (b) and (c) were 405 and 488 nm, respectively, and the corresponding emissions were collected at 425–575 nm (Hoechst) and 530–580 nm (NI-βGal). Scale bar = 20 μm. Representative images from repeated experiments are shown.

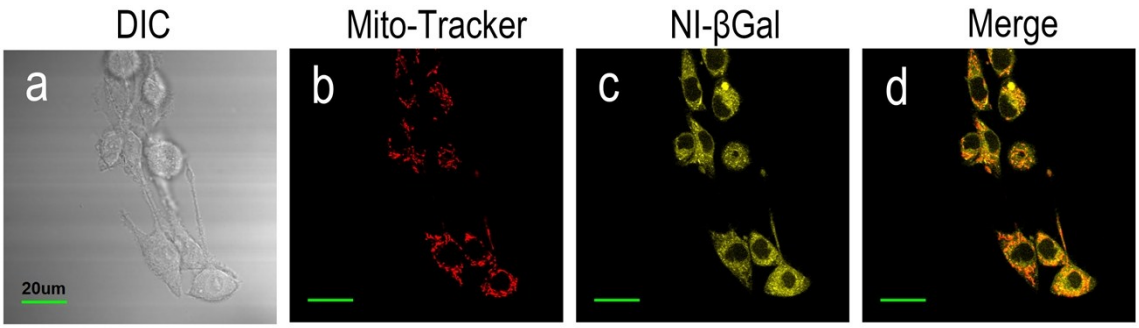

Fig. S16 Images of C6/lacZ7cells colabeled with (b) Mito-Tracker Deep Red and (c) NI-βGal. (a) DIC image. (d) Merged image of (b) and (c). The excitation wavelengths for (b) and (c) were 635 and 488 nm, respectively, and the corresponding emissions were collected at 650–700 nm (Mito-Tracker Deep Red) and 520–570 nm (NI-βGal). Scale bar = 20 μm. Representative images from repeated experiments are shown.

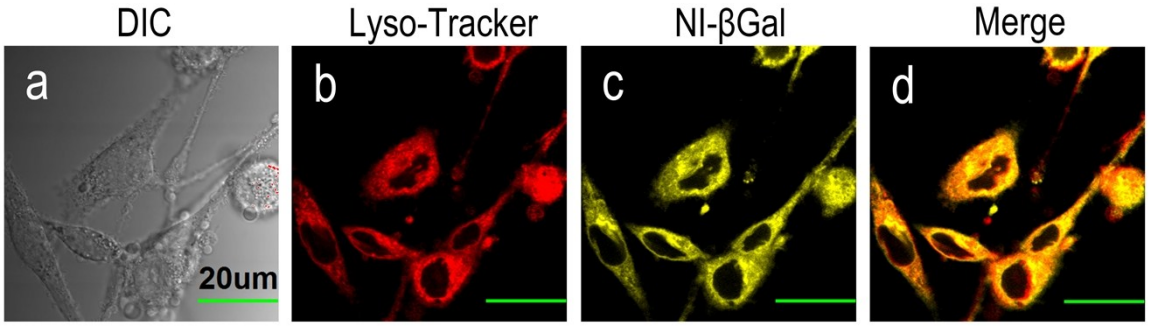

Fig. S17 Images of C6/lacZ7cells colabeled with (b) Lyso-Tracker Red and (c) NI-βGal. (a) DIC image. (d) Merged image of (b) and (c). The excitation wavelengths for (b) and (c) were 543 and 405 nm, respectively, and the corresponding emissions were collected at 580–600 nm (Lyso-Tracker Red) and 520–560 nm (NI-βGal). Scale bar = 20 μm. Representative images from repeated experiments are shown.

Vibrational Circular Dichroism (VCD) Experiment

To confirm the absolute configuration of NI-βGal Tetraacetate (**4**) or NI-βGal, namely α, β or both configurations (the last case means diastereomer mixture), vibrational circular dichroism (VCD) experiment was implemented at room temperature with ChiralIR-2X (BioTools, USA). The VCD spectrum of **4** was measured for 6 h using 0.04 M solutions of **4** in $CDCl_3$. Since two strong absorption bands 1050–1100 cm^{-1} and 1220–1280 cm^{-1} are the characteristic IR absorption for aryl alkyl ethers (C-O-C bond, whose orientation determines whether α or β-configuration of **4** herein), the resulting VCD spectrum of **4** in the frequency range 900–1350 cm^{-1} is shown in Fig. S20b. On the other hand, theoretical calculation was conducted with Gaussian 09[4] at the B3LYP/6-31G(d) DFT level using PCM solvation model. Two conformers of **4** in the β-configuration were determined from the relaxed potential energy surface scan for different relative orientation of pyran ring and naphthalene ring while allowing the geometry of the rest of the molecule to optimize. The conformers **a** and **b** in the β-configuration represent well defined local minima on the potential energy surface, as shown in Fig. S18. The relative populations of these two conformers were calculated on the basis of Boltzmann distribution law (Table S2). Vibrational frequencies, IR and VCD intensities were calculated for both conformers **a** and **b** of the β-configuration isomer. The results were analysed by multiwfn software[5] and the sum of the calculated spectra of conformers **a** and **b** weighted by their Boltzmann populations ([**a**]*0.936+[**b**]*0.064) were shown in Fig. 20c,d. Using the same method, only one conformer of **4** in the α-configuration was determined (Fig. S19) and its spectra were shown in Fig. 20e,f. Comparison of the observed spectra of **4** and theoretically calculated spectra of **4** in α or β-configuration revealed that **4** did exist predominantly in the β-configuration.

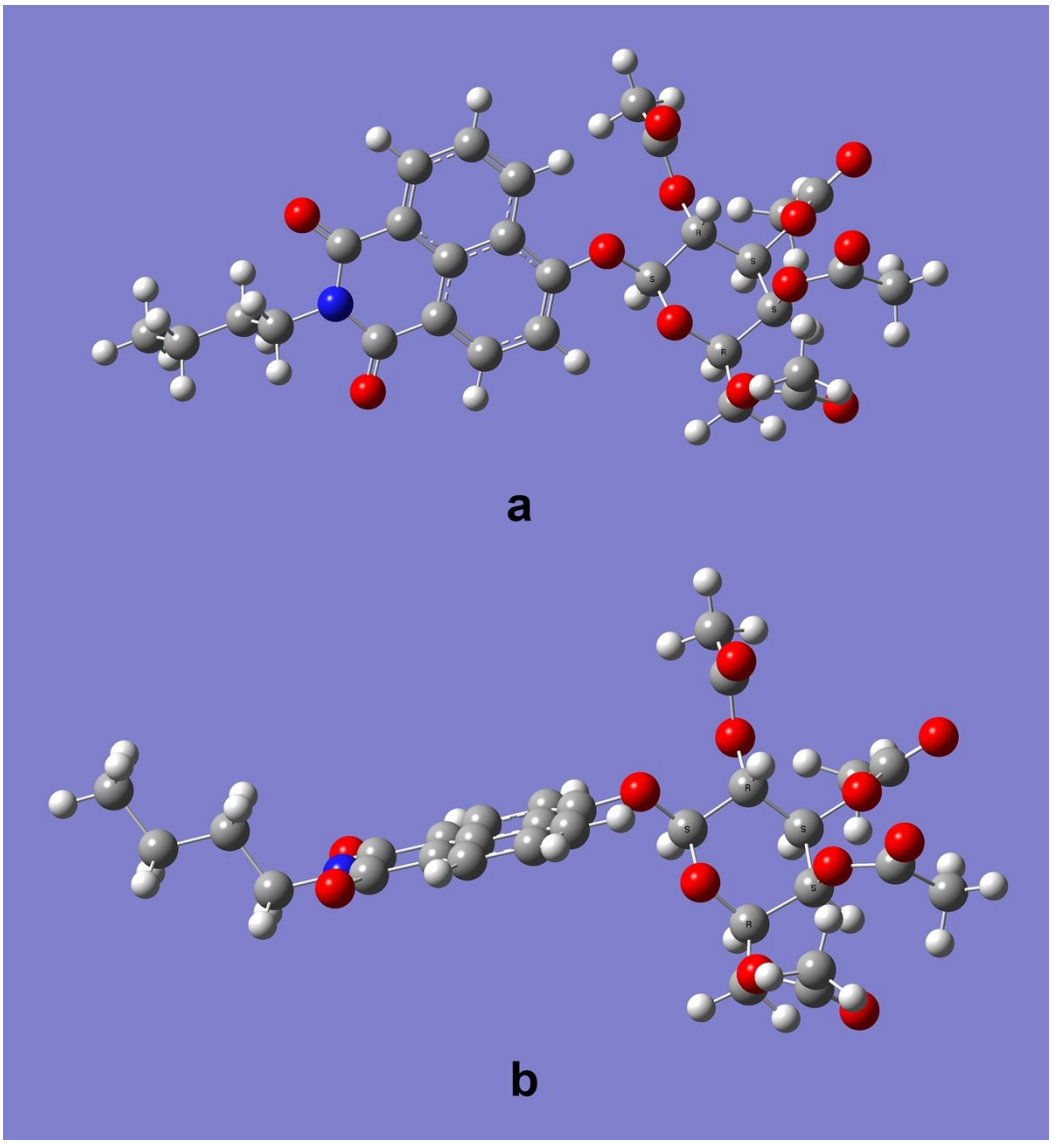

Fig. S18 Optimized geometries of the two lowest energy conformers in the β-configuration, **a** and **b**.

Table S2. B3LYP/6-31G(d) relative energies, relative free energies and populations of the conformations of NI-βGal Tetraacetate (**4**).

Conformer	ΔE [a]	ΔG [a]	$P(\%)$ [b]
a	0.00	0.00	93.6
b	2.47	1.59	6.4

[a] ΔE and ΔG in kcal mol^{-1}. [b] Populations based on ΔG values, T = 298.15 K.

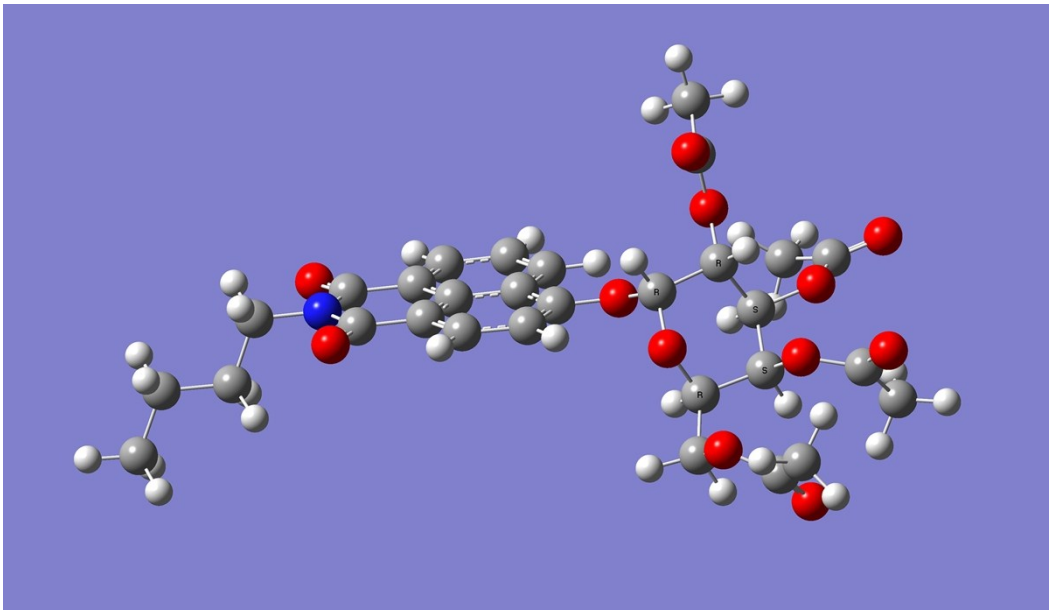

Fig. S19 Optimized geometry of the lowest energy conformer in the α-configuration.

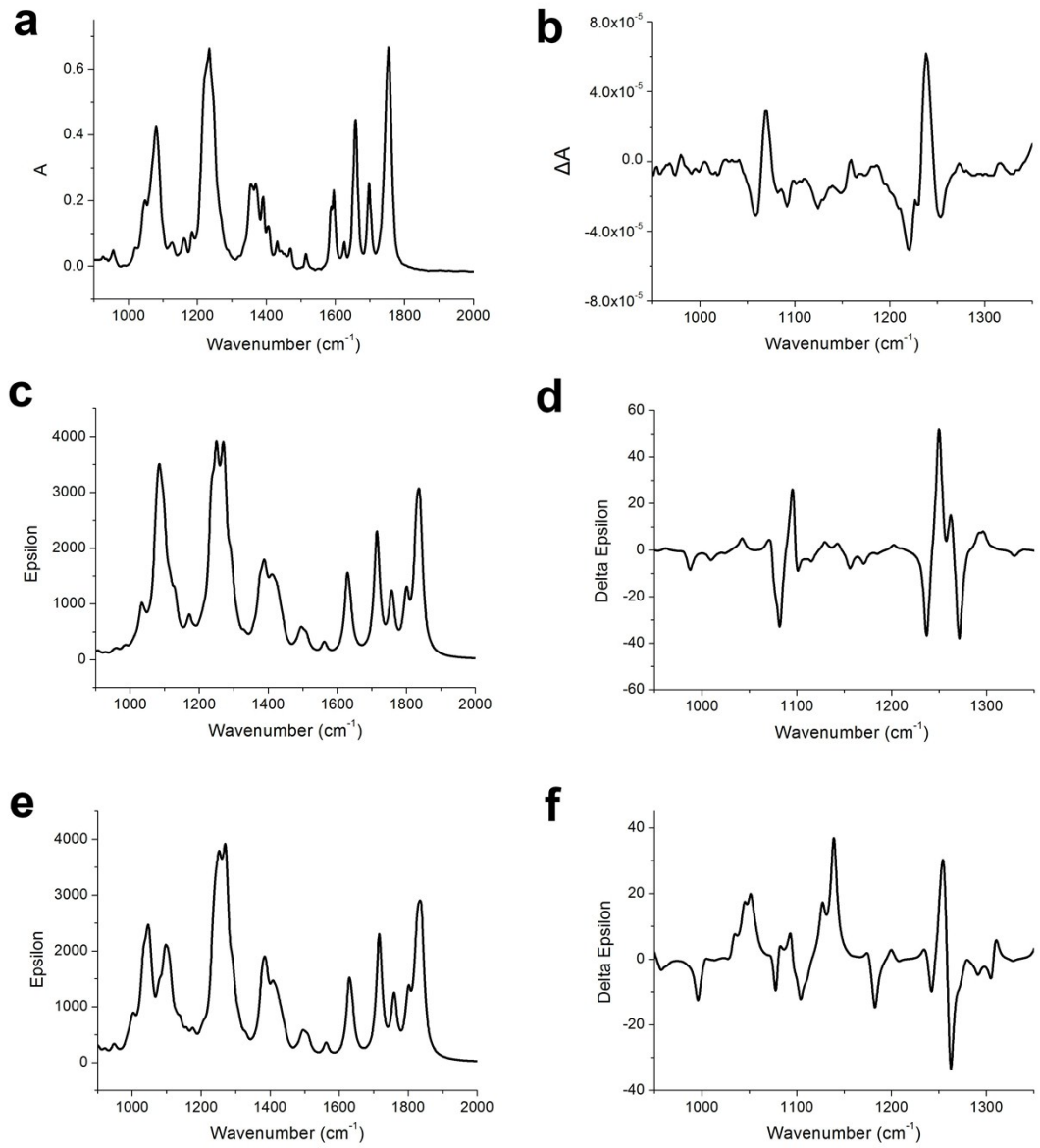

Fig. S20 (a,c,e) Experimentally observed IR spectra (a) of **4** and theoretically calculated IR spectra of **4** in the (c) β or (e) α-configuration. (b,d,f) Experimentally observed VCD spectra (b) of **4** and theoretically calculated VCD spectra of **4** in the (d) β or (f) α-configuration.

^{1}H NMR, ^{13}C NMR and HRMS data

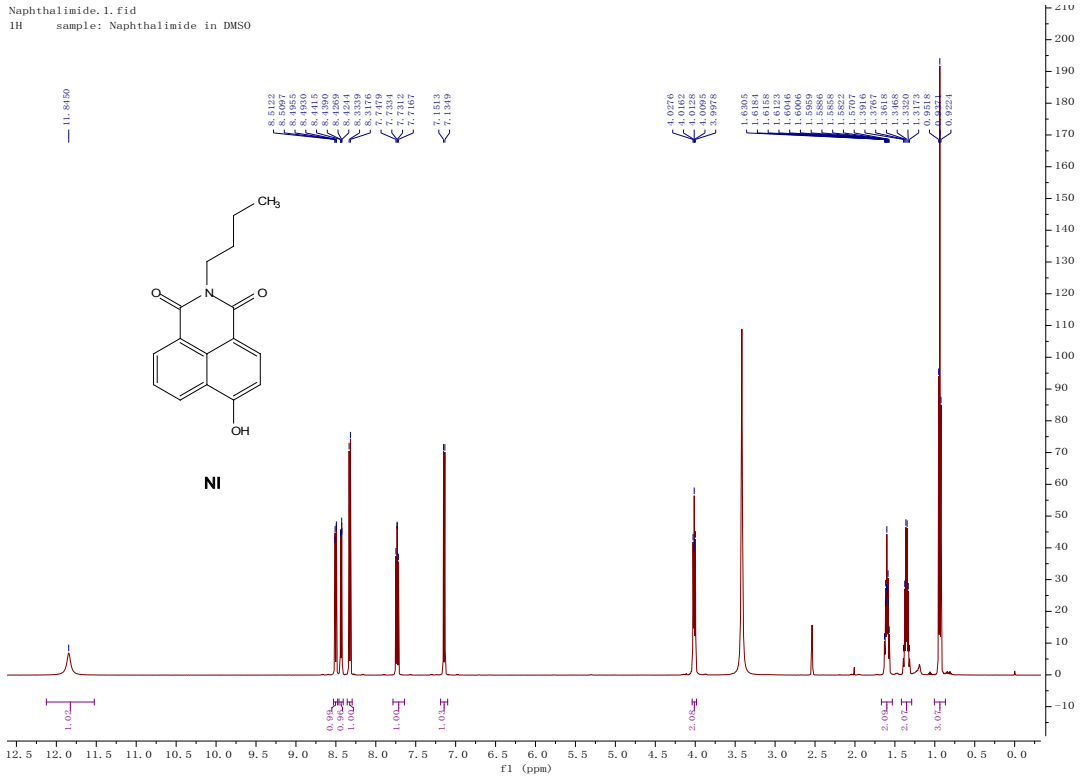

Fig. S21. ^{1}H NMR spectrum (500 MHz) of NI in DMSO.

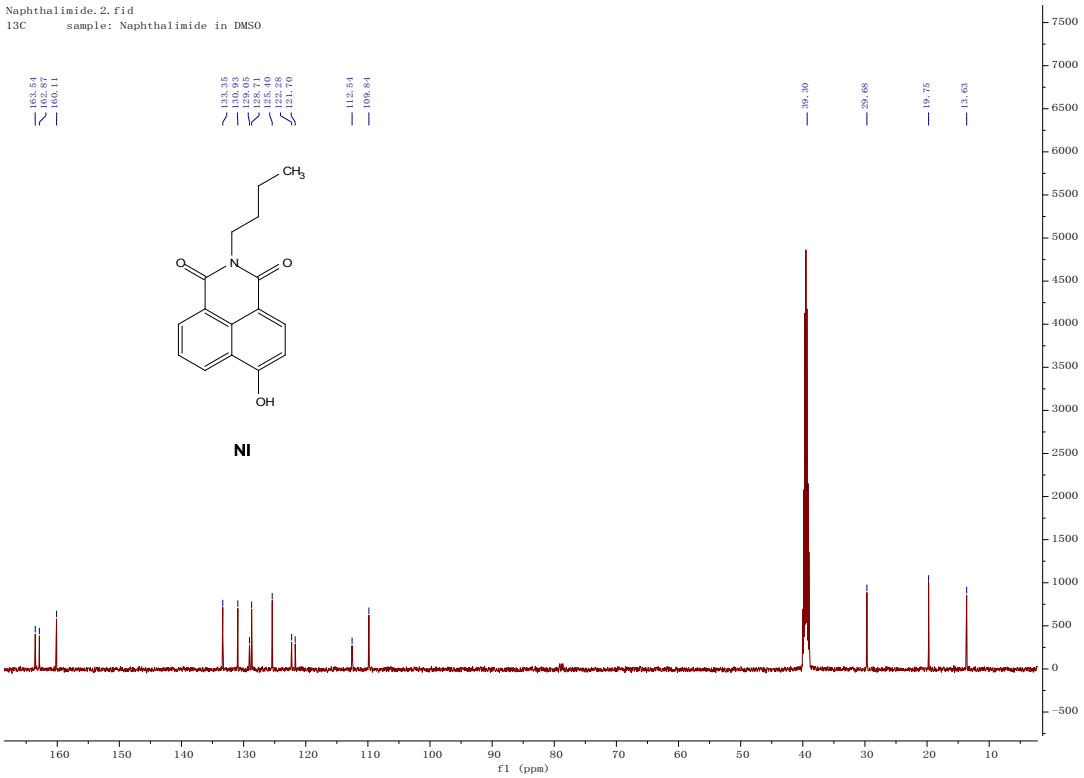

Fig. S22. ^{13}C NMR spectrum (126 MHz) of NI in DMSO.

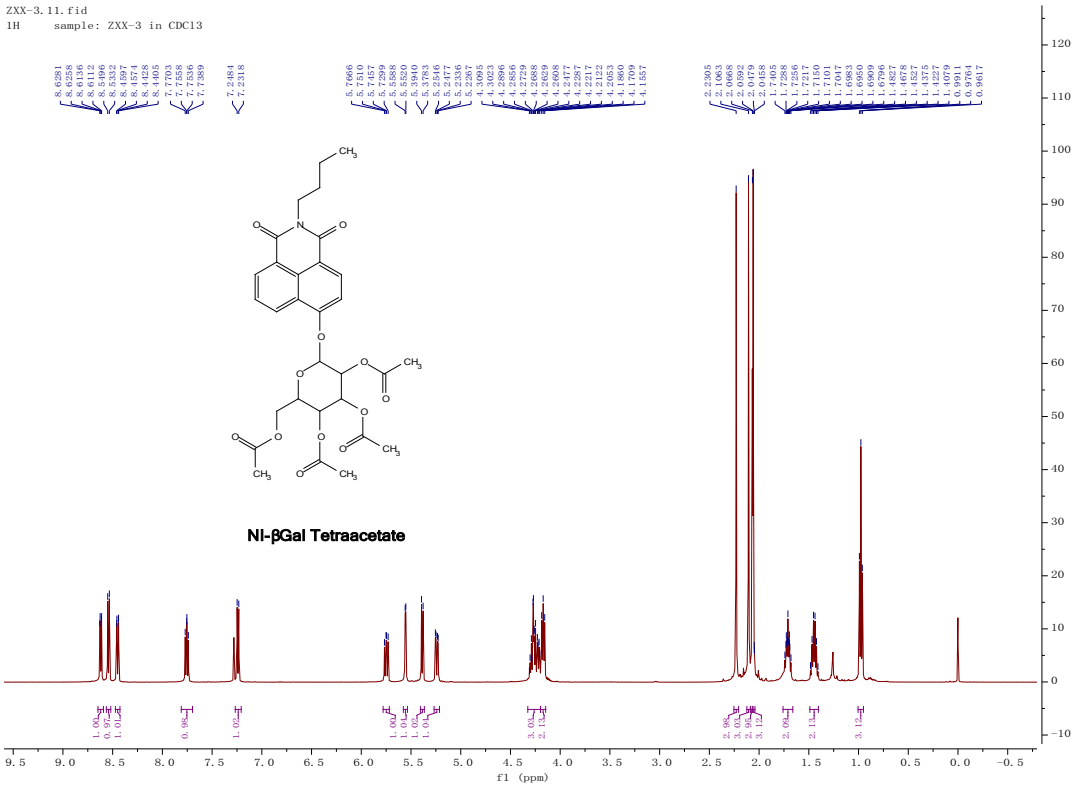

Fig. S23. ^{1}H NMR spectrum (500 MHz) of NI-βGal Tetraacetate in $CDCl_3$.

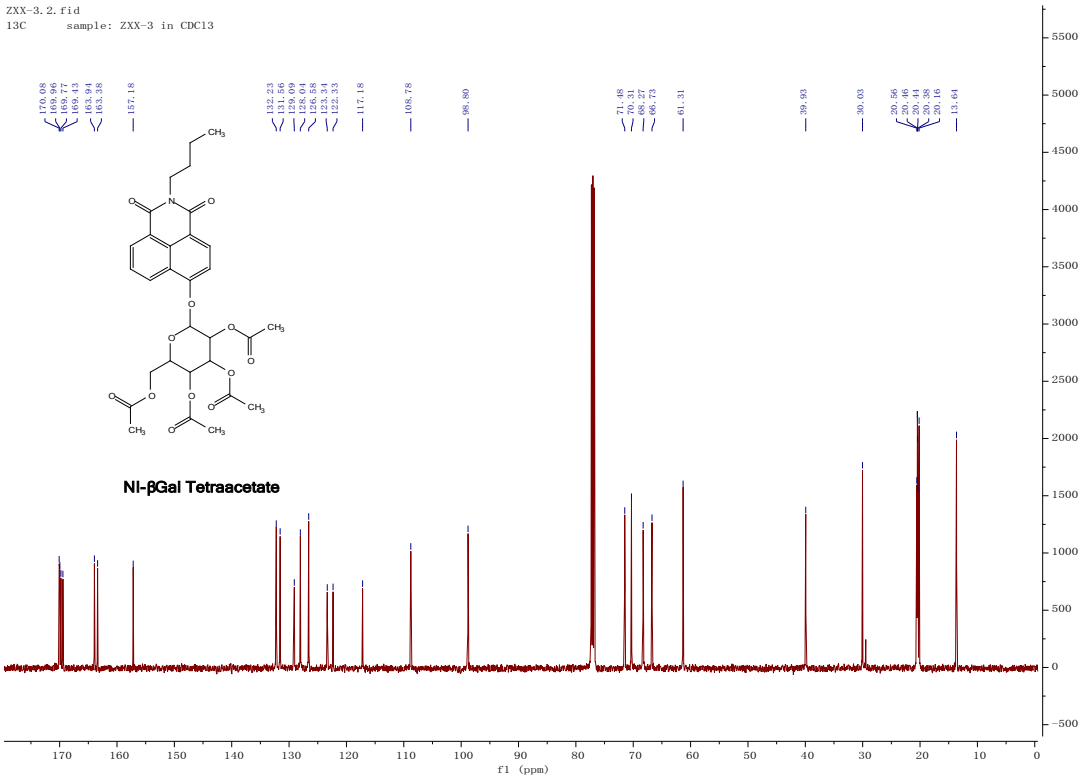

Fig. S24. ^{13}C NMR spectrum (126 MHz) of NI-βGal Tetraacetate in $CDCl_3$.

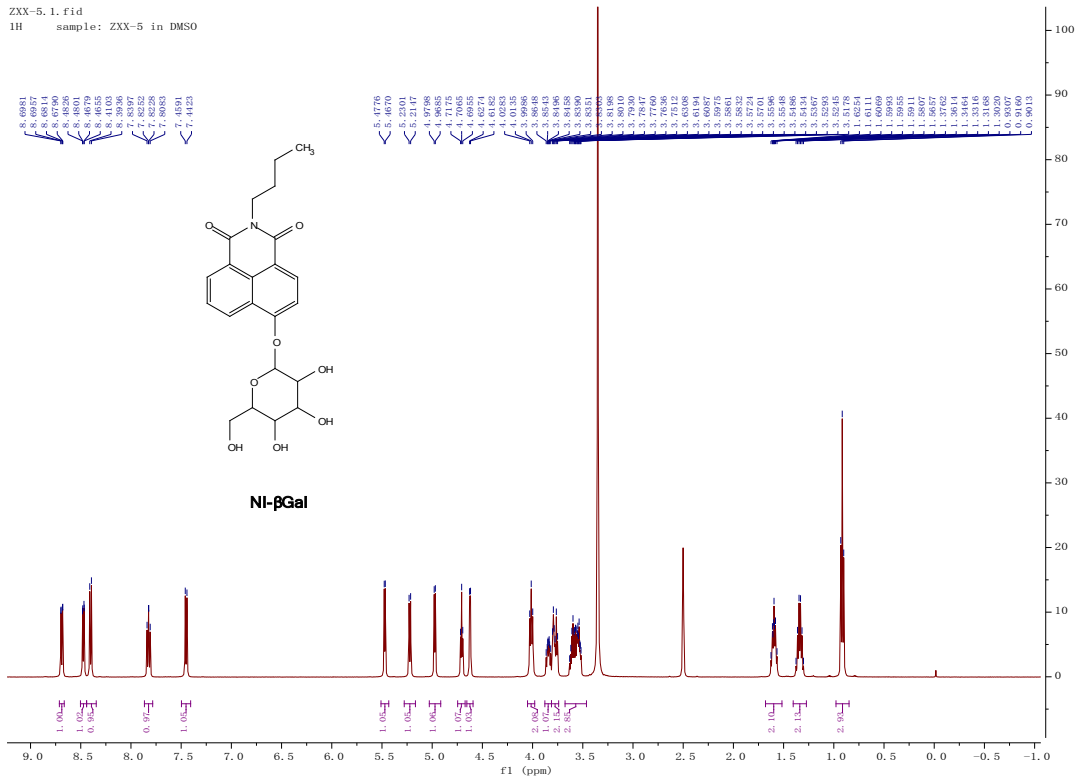

Fig. S25. ^{1}H NMR spectrum (500 MHz) of NI-βGal in DMSO.

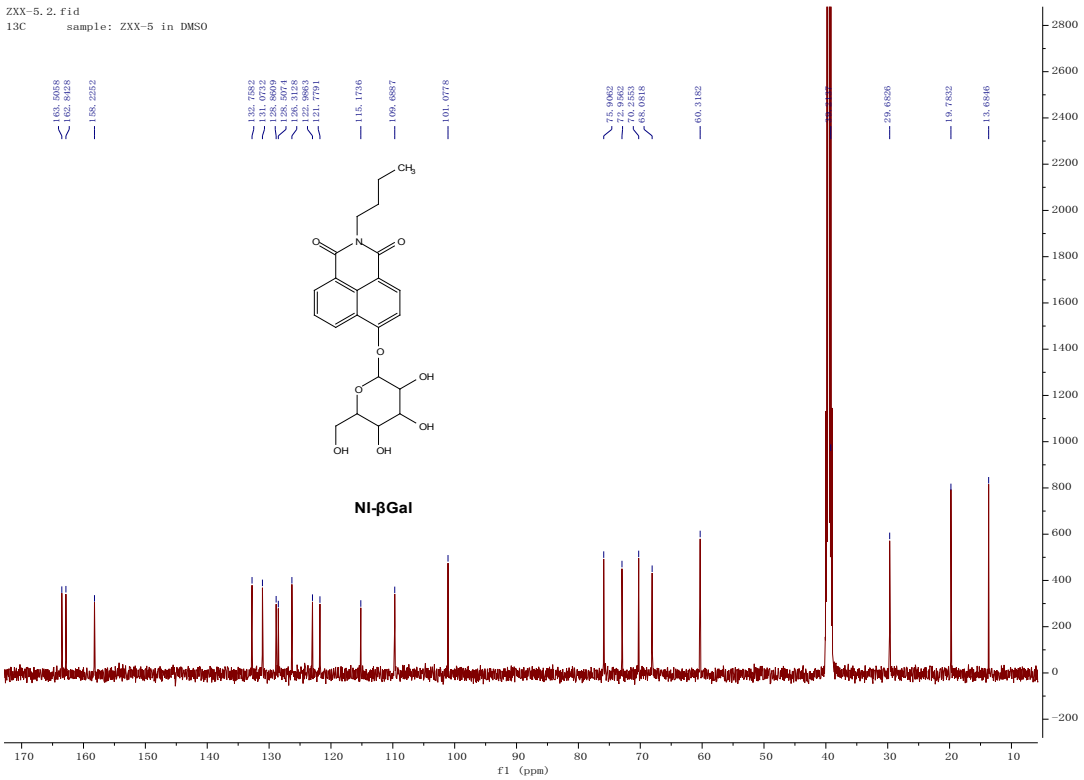

Fig. S26. ^{13}C NMR spectrum (126 MHz) of NI-βGal in DMSO.

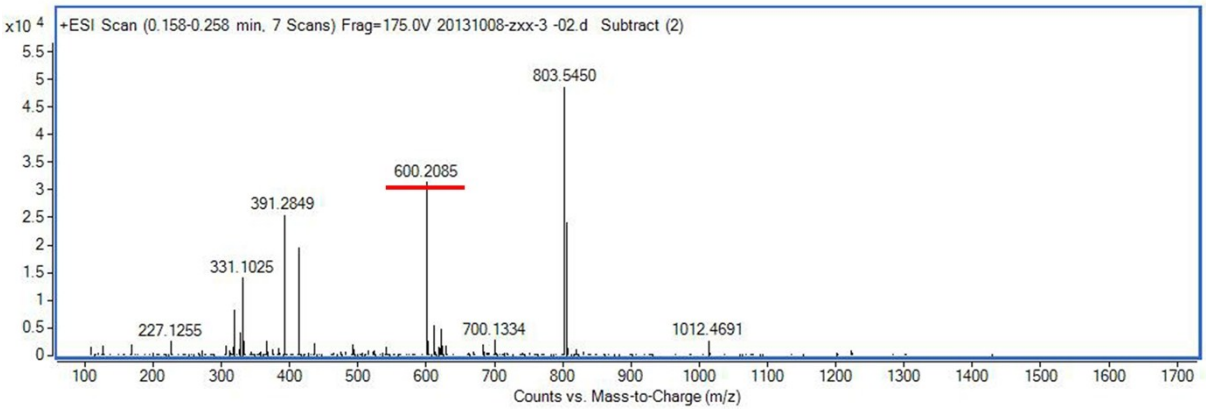

Fig. S27. HRMS (ESI$^+$) of NI-βGal Tetraacetate.

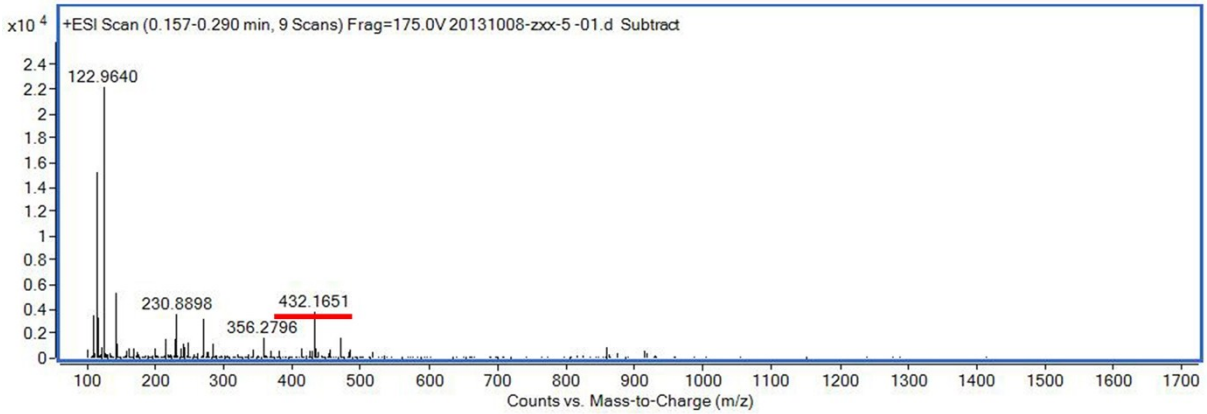

Fig. S28. HRMS (ESI$^+$) of NI-βGal.

References

1. R. F. Chen, *Anal. Biochem.*, 1967, **19**, 374–387.
2. Q. He, J. Shi, X. Cui, J. Zhao, Y. Chen and J. Zhou, *J. Mater. Chem.*, 2009, **19**, 3395–3403.
3. S. K. Bae, C. H. Heo, D. J. Choi, D. Sen, E. H. Joe, B. R. Cho and H. M. Kim, *J. Am. Chem. Soc.*, 2013, **135**, 9915–9923.
4. Gaussian 09, Revision B.01, M. J. Frisch, G. W. Trucks, H. B. Schlegel, G. E. Scuseria, M. A. Robb, J. R. Cheeseman, G. Scalmani, V. Barone, B. Mennucci, G. A. Petersson, H. Nakatsuji, M. Caricato, X. Li, H. P. Hratchian, A. F. Izmaylov, J. Bloino, G. Zheng, J. L. Sonnenberg, M. Hada, M. Ehara, K. Toyota, R. Fukuda, J. Hasegawa, M. Ishida, T. Nakajima, Y. Honda, O. Kitao, H. Nakai, T. Vreven, J. A. Montgomery, Jr., J. E. Peralta, F. Ogliaro, M. Bearpark, J. J. Heyd, E. Brothers, K. N. Kudin, V. N. Staroverov, T. Keith, R. Kobayashi, J. Normand, K. Raghavachari, A. Rendell, J. C. Burant, S. S. Iyengar, J. Tomasi, M. Cossi, N. Rega, J. M. Millam, M. Klene, J. E. Knox, J. B. Cross, V. Bakken, C. Adamo, J. Jaramillo, R. Gomperts, R. E. Stratmann, O. Yazyev, A. J. Austin, R. Cammi, C. Pomelli, J. W. Ochterski, R. L. Martin, K. Morokuma, V. G. Zakrzewski, G. A. Voth, P. Salvador, J. J. Dannenberg, S. Dapprich, A. D. Daniels, O. Farkas, J. B. Foresman, J. V. Ortiz, J. Cioslowski, and D. J. Fox, Gaussian, Inc., Wallingford CT, 2010.
5. T. Lu and F. Chen, *J. Comput. Chem.*, 2012, **33**, 580–592. http://multiwfn.codeplex.com/